Hyporheic exchange in gravel bed rivers with pool-riffle morphology: Laboratory experiments and three-dimensional modeling

Daniele Tonina[1,2] and John M. Buffington[3]

[1] We report the first laboratory simulations of hyporheic exchange in gravel pool-riffle channels, which are characterized by coarse sediment, steep slopes, and three-dimensional bed forms that strongly influence surface flow. These channels are particularly important habitat for salmonids, many of which are currently at risk worldwide and which incubate their offspring within the hyporheic zone. Here we perform a set of laboratory experiments examining the effects of discharge and bed form amplitude on hyporheic exchange, with surface-subsurface mixing measured directly from the concentration decay of a conservative tracer (fluorescein) injected into the surface flow. Near-bed pressure measurements were also used to predict hyporheic exchange from a three-dimensional pumping transport model. Comparison of the predicted and observed hyporheic exchange shows good agreement, indicating that the major mechanism for exchange is bed form–induced advection. However, the effect of bed forms is modulated by discharge and the degree of topographic submergence. We also tested the performance of the hydrostatic pressure as a proxy for the observed near-bed pressure in driving hyporheic exchange, which would facilitate field measurement and analysis of hyporheic flow in natural rivers. We found agreement with measured hyporheic exchange only for low bed form amplitudes and high flows.

Citation: Tonina, D., and J. M. Buffington (2007), Hyporheic exchange in gravel bed rivers with pool-riffle morphology: Laboratory experiments and three-dimensional modeling, *Water Resour. Res.*, *43*, W01421, doi:10.1029/2005WR004328.

1. Introduction

[2] The hyporheic zone is a band of permeable, saturated sediment surrounding a river, where surface water and groundwater mix, and includes riverbeds (shallow hyporheic zone), riverbanks, saturated sediments under dry bars (parafluvial hyporheic zone), and riparian and floodplain areas (floodplain hyporheic zone) [*Edwards*, 1998]. It is characterized by intense physical and chemical gradients due to the mixing of groundwater and surface water by upwelling and downwelling fluxes, which sustain an ecotone composed of benthic macroinvertebrates and fish [*Stanford and Ward*, 1993; *Gibert et al.*, 1994; *Williams and Hynes*, 1974]. The intensity and extent of hyporheic exchange is a function of flow interactions with the local channel topography [*Harvey and Bencala*, 1993; *Elliott and Brooks*, 1997a] and consequent spatial variation in the total near-bed pressure [*Vittal et al.*, 1977; *Savant et al.*, 1987] that drives subsurface flow.

[3] Previous studies have investigated hyporheic exchange in fine-grained, sand-bedded channels with two-dimensional dune and ripple bed forms, primarily through flume experiments and numerical simulations [*Savant et al.*, 1987; *Elliott and Brooks*, 1997a, 1997b; *Packman et al.*, 2000; *Marion et al.*, 2002]. Studies of hyporheic flow in coarse-grained rivers have also been conducted, mainly through field experiments and numerical models [*Bencala and Walters*, 1983; *Harvey and Bencala*, 1993; *Wondzell and Swanson*, 1996; *Haggerty et al.*, 2002; *Wörman et al.*, 2002; *Storey et al.*, 2003; *Gooseff et al.*, 2006]. However, few laboratory experiments of hyporheic flow have been conducted with gravel bed morphologies [*Cooper*, 1965; *Packman et al.*, 2004], and those that have been done, used simplified two-dimensional bed forms and well-sorted sediment [*Packman et al.*, 2004] (but see *Salehin et al.* [2004]).

[4] In this study, we examine hyporheic exchange in a set of laboratory experiments representative of natural gravel bed rivers with three-dimensional pool-riffle morphology [e.g., *Montgomery and Buffington*, 1997] (Figure 1) and with a heterogeneous substrate ranging from coarse gravel to fine sand, comparable to that found in mountain headwater streams used by spawning salmonids [*Kondolf and Wolman*, 1993; *Buffington et al.*, 2003, 2004]. We focus on this stream type because of its importance as habitat for salmonid species [*Montgomery et al.*, 1999; *Moir et al.*, 2004], many of which are currently at risk worldwide [*Nehlsen et al.*, 1991; *Montgomery*, 2003]. Salmon and trout bury their eggs in streambed gravels for incubation within the hyporheic zone. After hatching, the alevins live in the hyporheic zone before emerging into the stream [*Levy*

---

[1]Center for Ecohydraulics Research, University of Idaho, Boise, Idaho, USA.
[2]Now at Rocky Mountain Research Station, U.S. Forest Service, Boise, Idaho, USA.
[3]Rocky Mountain Research Station, U.S. Forest Service, Boise, Idaho, USA.

Figure 1. Example of low-flow experimental conditions: Exp1, 12.5 l s^{-1} discharge, 0.0041 m m^{-1} slope.

and Slaney, 1993]. Coarse-grained pool-riffle channels also differ from lower-gradient sand bed rivers in that they exhibit a wide range of flow regimes that change seasonally. Hence surface flow and the boundary conditions for driving hyporheic exchange tend to be more variable, which may cause temporal variations in the quality or quantity of hyporheic habitat.

[5] To address these conditions, we conducted a series of recirculating (closed system) flume experiments to examine hyporheic exchange in pool-riffle channels spanning a broad range of discharge and bed form geometry. We measured hyporheic exchange with a conservative tracer (fluorescein) that was added to the surface flow; the decay of the in-stream fluorescein concentration is a direct measure of the solute mass advected into the sediment and its dilution with subsurface pore water. We then compared the observed exchange to that predicted from a modified pumping transport model [after *Elliott and Brooks*, 1997b] that accounts for near-bed pressure distributions resulting from flow over three-dimensional bed forms. Finally, we investigated the performance of the pumping model using the hydrostatic pressure as a surrogate for the near-bed pressure, which, if successful, would facilitate field measurement and analysis of hyporheic flow in natural rivers.

2. Theory: Pumping Exchange Model

[6] Flow-boundary interactions in rivers generate spatial variations in near-bed pressure and hydraulic head gradients that drive advective pore water flow (hyporheic exchange) through porous sediments [*Ruff and Gelhar*, 1972; *Ho and Gelhar*, 1973; *Mendoza and Zhou*, 1992]. In particular, flow obstructions create an upstream high-pressure zone and a downstream low-pressure zone, resulting in hyporheic circulation under the object. In the same manner, bed forms, boulders, logs, or streambed irregularities created by biotic processes like salmon redds generate downwelling fluxes in which river water is forced into the streambed and banks in regions of high pressure, and complimentary upwelling fluxes in which subsurface water is expelled into the river in regions of low pressure [*Cooper*, 1965; *Thibodeaux and Boyle*, 1987]. This process of advective pore water flow is known as pumping exchange [*Elliott and Brooks*, 1997a, 1997b].

[7] *Elliott and Brooks* [1997a, 1997b] developed a two-dimensional pumping exchange model for sand bed rivers with dune-like bed forms. These two-dimensional bed forms have high relative submergence (small amplitudes compared to water depth) and create a longitudinal near-bed pressure distribution that can be approximated as a sinusoidal function [*Elliott and Brooks*, 1997a]. Furthermore, because the bed form volume is small relative to the total alluvial volume over which hyporheic flow occurs in these channels, the bed topography can be represented as a planar surface (retaining the bed form−induced sinusoidal pressure variation), without modeling hyporheic exchange through the bed forms per se [*Elliott and Brooks*, 1997a; *Packman et al.*, 2000; *Marion et al.*, 2002].

[8] In contrast, the bed morphology and flow in pool-riffle channels are strongly three dimensional [e.g., *Dietrich and Whiting*, 1989; *Carling*, 1992] and the longitudinal pressure distribution in these channels is not sinusoidal; rather, it varies in a complex manner in both the downstream and cross-channel directions. Consequently, it needs to be measured experimentally or predicted from computational fluid dynamics (CFD) software with appropriate closure. Moreover, pool-riffle bed forms have a large sediment volume and the planar bed approximation used in two-dimensional models may no longer hold.

[9] To address these issues, we propose a three-dimensional pumping model for driving hyporheic exchange (modified from *Elliott and Brooks* [1997a, 1997b]). We apply the model to a series of laboratory experiments in which the near-bed pressure is measured with an array of micropiezometers, and the hyporheic flow is predicted from these measurements, which form the boundary condition for a

Table 1. Hydraulic Characteristics of the Experiments

	Discharge, $1\ s^{-1}$	Bathymetry-Wetted Area (3-D Surface Area), m^2	Surface of Flowing Water (Horizontal Projection), m^2	Mean Water Depth, m	Mean Wetted Width, m	Mean Velocity, $m\ s^{-1}$	Water Surface Slope, m m^{-1}	Water Volume, m^3
Exp1	12.50	3.83	3.75	0.065	0.68	0.282	0.0041	3.3
Exp2	21.00	4.13	4.03	0.075	0.73	0.384	0.0041	3.4
Exp3	32.50	4.78	4.70	0.104	0.85	0.369	0.0018	3.8
Exp4	12.50	4.05	4.01	0.056	0.73	0.308	0.0041	3.1
Exp5	20.83	4.45	4.34	0.064	0.79	0.413	0.0041	3.2
Exp6	32.50	4.94	4.90	0.087	0.89	0.421	0.0018	3.7
Exp7	12.50	4.38	4.27	0.044	0.77	0.365	0.0041	2.8
Exp8	21.10	4.89	4.80	0.053	0.87	0.460	0.0041	2.9
Exp9	32.83	5.00	4.97	0.086	0.90	0.425	0.0018	3.5
Exp10	12.93	4.98	4.97	0.039	0.90	0.367	0.0041	3.0
Exp11	21.17	4.98	4.97	0.052	0.90	0.452	0.0041	3.1
Exp12	32.58	4.98	4.97	0.082	0.90	0.442	0.0018	3.4

finite element model of groundwater flow, described in section 3.4.

[10] We treat the hyporheic flow as groundwater flow through a porous medium using Darcy's law. The Darcy equation is typically written in terms of laminar pore flow (i.e., small Reynolds numbers, $Re \approx 1$) [*Hassanizadeh and Gray*, 1987] and locally uniform velocities, but can be modified for variable flow, where inertial terms start to influence the flow field [*Dagan*, 1979]. In our analysis, we assume laminar Darcy flow through a homogeneous and isotropic sediment, appropriate for the experimental conditions examined (section 3.3.4)

$$\mathbf{u} = -k\frac{\partial H}{\partial \mathbf{x}} \qquad (1)$$

where $\mathbf{u}$ is the Darcy velocity, $\mathbf{x}$ is the coordinate vector, k is the hydraulic conductivity of the sediment, and H is the energy head defined as the total pressure normal to the bed surface (both the dynamic and static components, expressed in meters of water) plus the elevation head (bed surface height above the datum).

[11] The proposed pumping exchange method is modified from *Elliott and Brooks* [1997a] by extending their model to a three-dimensional flow field and removing both the assumptions of a planar bed and a downstream sinusoidal pressure variation, which is replaced by the measured near-bed pressure. The sinusoidal pressure variation was employed by *Elliott and Brooks* [1997a] because it approximated the near-bed pressure distribution over two-dimensional dunes, but was not intended as a general solution for other bed topographies.

[12] The *Elliott and Brooks* [1997a] model is based on the average downwelling flux of river water and solute over the bed, $\overline{q}$, and the flux-weighted average residence time distribution of the tracer into the bed, *RTD*. Additionally, the solute mass exchange is related to the in-stream concentration, $C(t)$, by mass balance.

[13] The downwelling flux of solute into the streambed is calculated directly from the groundwater flow field at the bed surface

$$q(x,y) = \begin{cases} \mathbf{u}_b \cdot \mathbf{n} & if\ \mathbf{u}_b \cdot \mathbf{n} > 0 \\ 0 & if\ \mathbf{u}_b \cdot \mathbf{n} \leq 0 \end{cases} \qquad (2)$$

where $\mathbf{u}_b$ is the Darcy velocity at the boundary (positive entering the domain), and $\mathbf{n}$ is the unit vector orthogonal to the bed surface (positive pointing inward). The average flux is then calculated over the bed form–wetted bathymetry, W_p (three-dimensional surface area of wetted topography). The *RTD* is defined as

$$RTD(t) = \frac{1}{W_p\overline{q}} \int_0^L \int_0^{P_H(x)} q(x,y) R_T(t,x,y) dx dy \qquad (3)$$

where $P_H(x)$ is the wetted perimeter, which is a function of the longitudinal position, L is the total length of the experimental reach, and R_T is the cumulative probability that a tracer entering the bed at position (x, y) (Cartesian coordinates) at time t_0 (set equal to 0) will remain in the bed later than a given time t, described by the relation

$$R_T(t,x,y) = \begin{cases} 1 & t \leq T \\ 0 & t > T \end{cases} \qquad (4)$$

where T is the residence time associated with the injection point (x, y). Values of R_T were determined using the forward particle tracking method, in which a set of particles is released at the sediment surface [*Tompson and Gelhar*, 1990]. Hence the particle moves in short time intervals with the local velocity, and its pathline can be tracked, and the relative residence time computed.

[14] The average depth of solute penetration, m_e, is assessed by convoluting the average downwelling flux by the equation

$$m_e(t) = \frac{1}{C(t)} \int_0^t \overline{q} RTD(\tau) C(t-\tau) d\tau \qquad (5)$$

where at a given time step, t is constant and τ is a dummy time variable of integration. For a recirculating flume experiment, where the sediment is initially saturated with water, and a tracer of initial concentration C_0 is homogeneously mixed into the surface flow, the mass balance between in-stream water and pore water is

$$\frac{C(t)}{C_0} = C^*(t) = 1 - \frac{W_p\varphi}{V_w} m_e(t) \qquad (6)$$

Table 2. Pool-Riffle Characteristics Per Experiment

	Volume of Sediment,[a] m^3	Dry Bar Volume, m^3	Bed Form Amplitude Δ, m	Ratio Δ/λ
Exp1	1.486	0.044	0.12	0.022
Exp2	1.486	0.028	0.12	0.022
Exp3	1.486	0.002	0.12	0.022
Exp4	1.471	0.018	0.09	0.016
Exp5	1.471	0.009	0.09	0.016
Exp6	1.471	0	0.09	0.016
Exp7	1.469	0.007	0.06	0.011
Exp8	1.469	0.001	0.06	0.011
Exp9	1.469	0	0.06	0.011
Exp10	1.464	0	0.036	0.007
Exp11	1.464	0	0.036	0.007
Exp12	1.464	0	0.036	0.007

[a]Mean sediment depth of all experiments is approximately 0.3 m.

where V_w is the total volume of water present in the system, except for the pore water, and φ is the sediment porosity. C^* is the in-stream concentration normalized by the initial value, C_0. Simultaneous solution of equations (5) and (6) gives the in-stream solute concentration $C(t)$.

3. Methods

[15] To study hyporheic exchange and analyze the mechanisms of solute transfer in gravel pool-riffle channels, a set of twelve experiments in a recirculating flume was conducted with uniform flow and constant discharge (Table 1). A sand and gravel mixture was molded into a uniform pool-riffle morphology, with four sets of bed form amplitudes examined, and three discharges for each set, simulating a range of natural channel conditions (Table 2). The following sections describe the details of our approach.

3.1. Pool-Riffle Morphology and Experimental Setup

[16] The pool-riffle morphology used in the experiments was designed to represent a natural headwater stream, although simplified to a regular sequence of alternate bars and pools in a single straight channel. For low discharges, the flow in pool-riffle channels meanders around the bars, accelerating over the riffles and diving into the pools (Figure 1). At high flow, the bars become submerged, limiting the horizontal flow displacement. The wavelength and amplitude of pool-riffle topography depends on discharge, flow history [*Tubino*, 1991], sediment size and grading [*Lanzoni and Tubino*, 1999], and presence of externally imposed flow obstructions (wood, bedrock outcrops, etc.) [*Buffington et al.*, 2002].

[17] Our experiments examine a straight channel, without obstructions, having alternate bars and a pool-to-pool spacing of six channel widths. Self-formed pool-riffle channels typically have a mean pool wavelength (λ) of about five to seven bankfull widths [*Leopold et al.*, 1964; *Keller and Melhorn*, 1978], although values as low as three channel widths have been reported [*Carling and Orr*, 2000]. The residual pool depth, defined as the difference in elevation between the riffle crest and the pool bottom [*Lisle and Hilton*, 1992], determines the pool-riffle amplitude, Δ, which is half of the total amplitude between pool bottom and bar top in a topographically symmetrical channel. In this study, we define bankfull depth as the water depth that completely submerges the highest bed form, and we examined four bed form amplitudes (0.12, 0.09, 0.06, 0.036 m), corresponding to residual pool depths of 1, 0.75, 0.5 and 0.3 times the reach-average bankfull depth (referred to as large, medium, low and small bed form amplitude, respectively). With a constant bed form wavelength (5.52 m), the ratio of bar amplitude to wavelength, Δ/λ, takes values of 0.022, 0.016, 0.011, and 0.007 in our study (Table 2), which cover typical ranges for self-formed pool-riffle channels [*Prestegaard*, 1983; *Buffington and Montgomery*, 1999]. The basic shape of the bed topography was predicted from the weakly nonlinear theory of *Colombini et al.* [1987] and *Tubino* [1991], adjusted for grain heterogeneity by *Lanzoni and Tubino* [1999]. The predicted topography

Figure 2. Pool-riffle bed form, with an amplitude-to-wavelength ratio (Δ/λ) of 0.0215, largest amplitude.

Figure 3. Process of pool-riffle construction using wooden ribs to mold bed topography.

was then modified for the desired bed form amplitude of each experiment.

[18] The experiments were conducted at the Saint Anthony Falls Laboratory in their tilting flume, which is 14.6 m long, 0.9 m wide and 0.6 m deep. The experimental bed was 13.92 m long, over which a pool-riffle topography was shaped by hand, comprising a 2.5λ long section (Figure 2). A series of wooden ribs was used to mold the desired cross-sectional shape of the channel for each experiment (Figure 3). To change the bed form amplitude, the riffle crest was held at a constant height of 30 cm, while the bar top and pool concavity were adjusted to obtain the desired bed form topography. Sediment depths were shallowest below the pool, ranging from 18 to 26 cm for the largest and smallest bed form amplitudes, respectively. Figure 2 shows the final bed shape for the largest amplitude.

[19] The sand and gravel sediment mixture used in the experiments ranged from <1 to 27 mm, with a median grain size of approximately 10 mm (Figure 4). This grain size distribution is within the range used by spawning salmonids, albeit on the fine side of what is typically preferred [*Kondolf and Wolman*, 1993]. The amount of fine particles (sizes <6.4 mm) used in the experiments was chosen to match the threshold for successful survival to emergence of salmonid fry (90% survival when fines comprise $\leq$20% of the sediment distribution [*Bjornn and Reiser*, 1991]).

3.2. Discharge and Slope

[20] We examined three discharges for each bed form amplitude (Tables 1 and 2). The first two discharges were 12.5 and 21 l s^{-1}, simulating low discharges where the flow meandered around the bars. Low discharges of this sort are important because they are the most common flow in mountain rivers and are typical conditions during spawning activity of many salmonids. The third discharge submerged the entire bed topography to a flow height close to the bar tops, representing a high-flow event with a discharge of 32.5 l s^{-1} (Figure 5). The flume was adjusted to two slopes: a steeper slope of 0.0041 m m^{-1} used for the low dis-

charges, and a lower slope of 0.0018 m m^{-1} used for the largest flow. The lower slope was chosen in order to submerge the bed at high flow. Water was recirculated during the experiments, and the flume was lined with a thin plastic sheeting to prevent water leakage. Except for minor surface winnowing of fine grains, the sediment was not mobilized by the imposed flows (section 3.3.3).

3.3. Measurements

[21] We instrumented only one pool-to-pool sequence because the topography was periodic and the flow conditions were similar over each sequence. These results were then extended over the entire experimental domain (Figure 6).
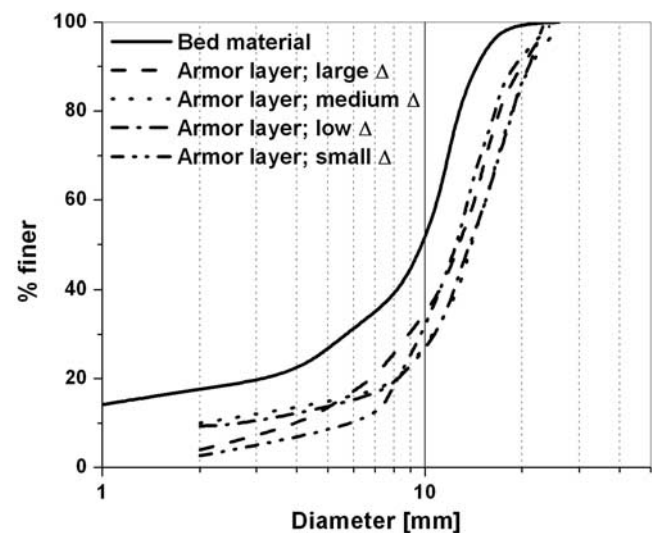

Figure 4. Grain size distribution of the sediment mixture used in the experiments (solid line) and that of the armor layer developed over the riffle area for each bed form amplitude (Δ, Table 2) (dashed, dotted, dash-dotted, and dash-double-dotted lines).
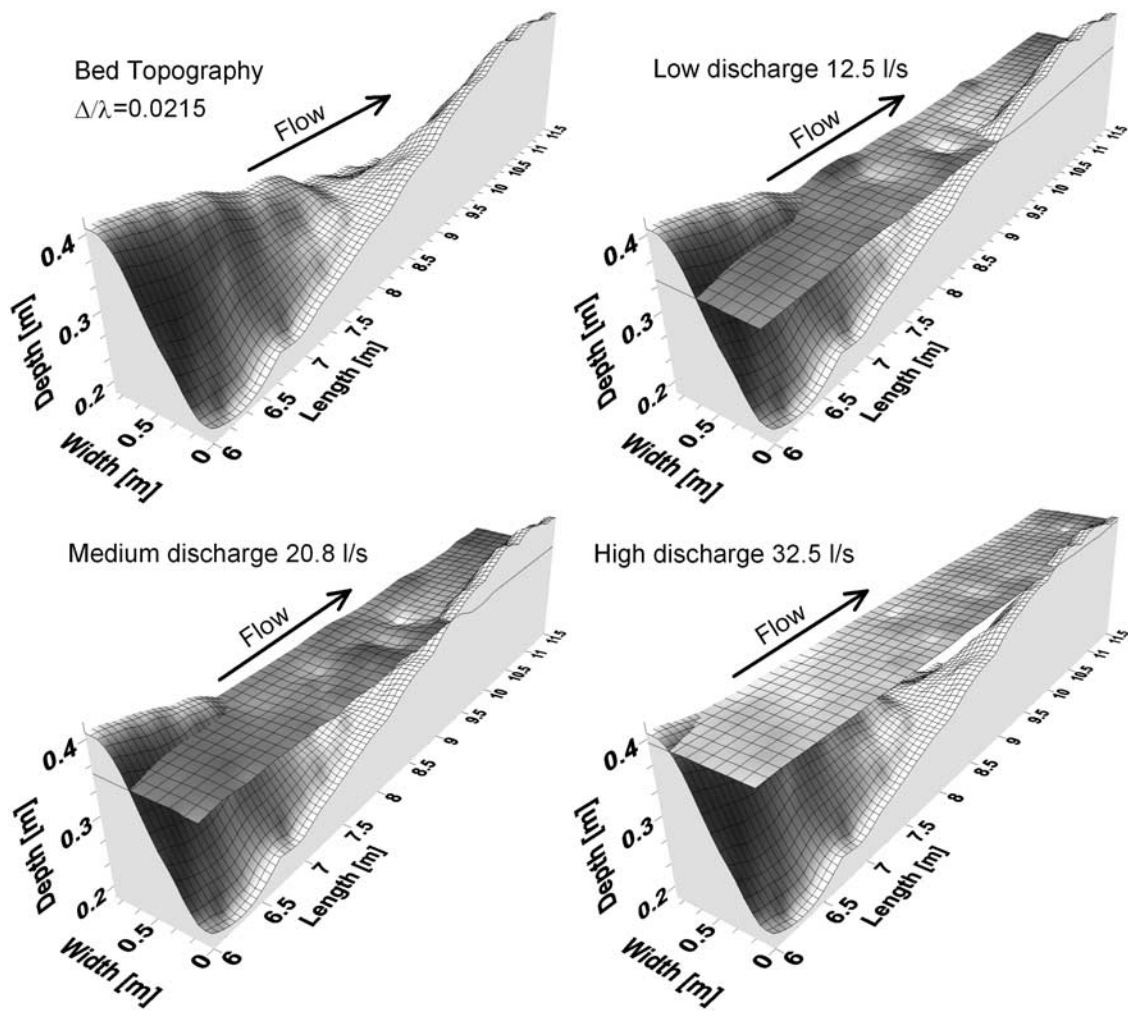
Figure 5. Pool-riffle topography for the largest bed form amplitude ($\Delta/\lambda = 0.0215$), showing the degree of submergence and water surface topography for three different discharges.

The monitored reach was located between cross sections 26 and 49 (Figure 6).

3.3.1. Pressure Measurements

[22] The pressure distribution at the bed surface was measured with micropiezometers composed of superthane (ether) tubes (1/16″ inside diameter and 1/8″ outside diameter) (Figure 7). The surface piezometers had a longitudinal spacing of 72 cm and were placed in cross-sectional sets as shown in Figure 6 (lateral spacing of approximately 10 cm). Nests of subsurface piezometers were also placed at the end points of the monitored reach (cross sections 26 and 49; see Figure 6). The subsurface piezometers had a 10 cm lateral spacing and a 6 cm vertical spacing.
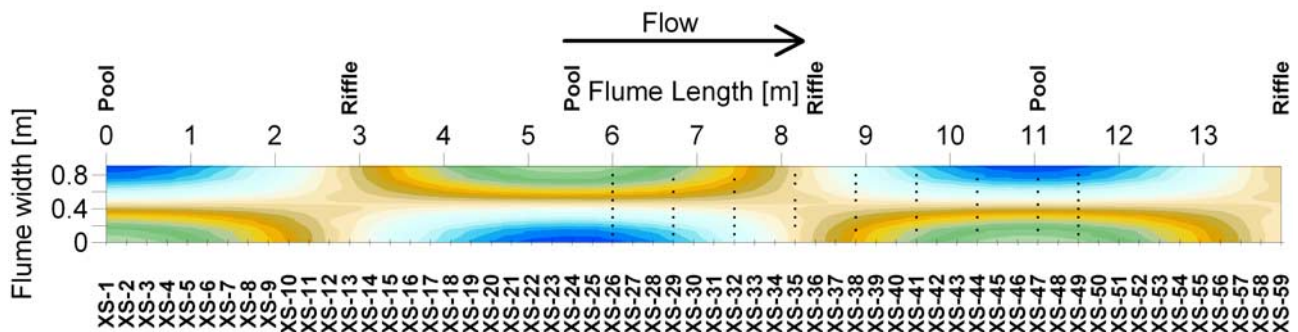

Figure 6. Shaded relief plan view of pool-riffle bed topography; blue areas correspond to pools and green areas to bar tops. The monitored reach is between XS 26–49, and the dots indicate locations of surface micropiezometers.

Figure 7. Photograph of a micropiezometer for measuring pressure at the sediment-water interface.

[23] The surface piezometers were placed flush with the sediment surface to minimize disturbance of the flow and were installed during the molding of the bed topography. Because of the small diameter of the tube, a capillary rise was measured and subtracted from the recorded values. The water height in the tubes was gauged using calipers, with an estimated maximum measurement error of approximately 1 mm.

[24] Measuring spatial variations in the near-bed pressure is laborious in natural channels with complex topography [*Baxter and Hauer*, 2000]. However, the hydrostatic pressure may approximate the actual near-bed pressure under certain circumstances, and is considerably easier to measure. We expect that the hydrostatic pressure will be a useful proxy when the dynamic pressure and associated turbulent losses are minimized, such as for gradually varying flow (typical of self-formed pool-riffle channels, where gradually varying topography minimizes flow separation in the lee of bed forms) or when the hydrostatic head variations are larger than the dynamic ones. We examined this issue by comparing the hyporheic flux predicted from the observed near-bed pressure versus that of the hydrostatic pressure.

[25] The hydrostatic pressure was determined from measurements of the bed topography and water surface elevation. These values were measured using a manual point gauge mounted on a trolley fixed to the flume. The topography and water elevation for each discharge were measured to the nearest half millimeter (or to the nearest millimeter for wavy water surfaces (section 5.1)) on a grid with a transverse spacing of 10 cm and a longitudinal spacing of 24 cm.

3.3.2. Conservative Tracer

[26] Fluorescein was used as a tracer to assess solute exchange between in-stream water and subsurface pore water. The advantages of fluorescein are a small temperature coefficient (-0.36% per $°C$) and detection at very low concentrations (10 parts per trillion), but direct sunlight rapidly destroys it. Because the experiments were conducted in a laboratory flume with very low sunlight and no direct exposure, the latter effect is negligible.

[27] We used a flow-through cell 10-AU Fluorometer (Turner Designs, Inc.) to measure the fluorescein concentration, corrected for temperature changes during the experiments. The fluorometer was calibrated between the fluorescence of the tap water used to fill the flume and the expected fluorescein concentration present in the flume at the initial condition after injection of the tracer. Concentration values were averaged every eight seconds and logged every ten seconds.

[28] Additionally, sodium chloride (NaCl) was used as an alternative passive tracer, but the measured conductivity underestimated the NaCl concentration at the tails of the concentration curve; therefore the NaCl measurements were not used in the analysis. Nevertheless, the NaCl tracer accurately recorded the bulk of the hyporheic exchange in these coarse, porous sediments [*Tonina*, 2005] and may be a useful tracer for field studies of other porous sediments where rapid exchange rates occur, and for those studies where quantification of the tail of the concentration curve is not required.

3.3.3. Surface Grain Size and Armor Layer

[29] After each set of experiments (and before changing the bed morphology), a surface pebble count [*Wolman*, 1954] was made to assess the grain size distribution of the surface material. The monitored reach was divided into three zones (riffle, pool, and bar), with 150 particles randomly selected from each zone. We then assessed the thickness of the armor layer by digging several holes and measuring the depth of armoring. A weak armor layer developed through surface winnowing of fine grains (Figure 4), but the rest of the bed remained immobile for the imposed discharges.

3.3.4. Hydraulic Conductivity of the Sediment

[30] Hydraulic conductivity is a function of the material composition, grain packing, and orientation of the particles. In placing the sediment, care was taken to create a matrix with fairly homogeneous and isotropic hydraulic properties. This was done to provide experimental control, however we recognize that natural channels can be substantially more complex, having heterogeneous sediment mixtures that are commonly anisotropic and possibly influenced by organic matter. These natural complexities can significantly alter subsurface flow properties. At the end of the experiments, we dug transects into the sediments to verify that there was no settling of fine particles, or substantial heterogeneities. Because of the large requisite volume of material needed to characterize the conductivity of such coarse sediment, and to avoid potential bias caused by disturbing the sediment, we used the entire flume as a permeameter. To measure hydraulic conductivity, we flattened the bed, tilted the flume slope to 0.18%, and established a constant discharge through the bed without creating a free surface flow over the sediment. The hydraulic conductivity was then determined as

$$k = \frac{Q}{As_f} \qquad (7)$$

where Q is the measured discharge, A is the cross-sectional area of saturated sediment, and s_f is the flume slope (representing the energy gradient). The hydraulic conductivity was found to be 5 cm s^{-1}, within the typical range for this type of material [*Freeze and Cherry*, 1979].
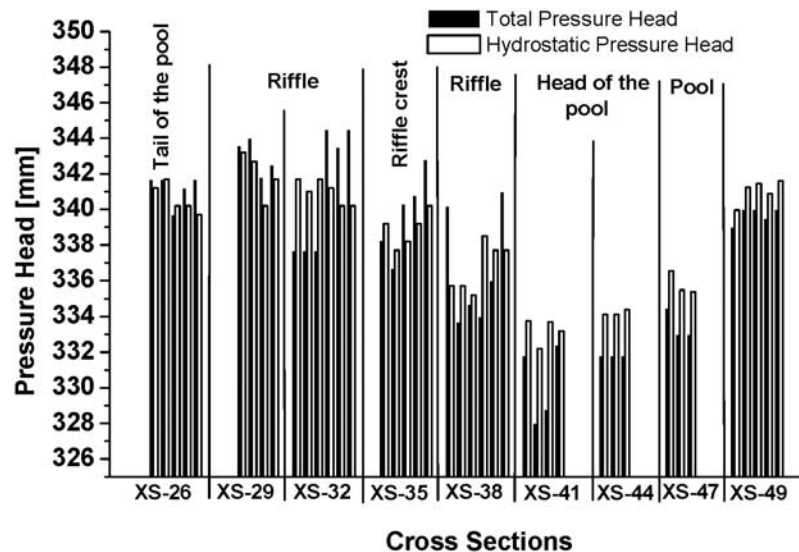
Figure 8. Comparison of near-bed total pressure versus hydrostatic pressure for Exp1 (large-amplitude bed form, low discharge). Pressures are reported from upstream to downstream and for each cross section from left to right across the channel, looking downstream (see Figure 6 for measurement locations). Empty space indicates exposed piezometers along the dry part of the bar.

3.4. Numerical Model

[31] The hyporheic flow was modeled using FLUENT 6.0 (FLUENT Inc.), a finite element CFD software package, which solved the Darcy equation for groundwater flow in the three-dimensional domain. Although, we preferred FLUENT for its flexibility in mesh generation, other software packages could be used, such as the well-known MODFLOW, which is a finite difference code that has been used in field studies of hyporheic flow [e.g., *Kasahara and Wondzell*, 2003; *Storey et al.*, 2003; *Cardenas et al.*, 2004; *Gooseff et al.*, 2006].

[32] The reach was meshed with a grid of approximately 3-cm-sided hexahedral elements. This dimension is larger than the size of sediment pores and, at the same time, is small compared to the domain size, allowing appropriate application of Darcy's law [*Hassanizadeh and Gray*, 1979]. Additionally, the quasi-uniform dimension of the elements produces a good quality mesh that satisfies the maximum principle; elements that are long and thin can create steep volume gradients and generate fictitious velocity profiles that are artifacts of a poorly constructed mesh. We also evaluated the sensitivity of the results to mesh size. Results varied by less than 3% when mesh dimensions were increased or decreased by 30%, which is consistent with FLUENT's definition of mesh independence.

[33] The study domain is defined by six boundary conditions: the two flume sidewalls and bottom, that were modeled as impervious layers (no-flow boundary), and the bed surface and vertical ends of the sediment volume, that were set in FLUENT as pressure inlet boundaries. When the bars were only partially submerged, a seventh boundary condition was needed, which is the water table below the partially submerged bars (treated as a no-flow boundary).

[34] Once the flow field was generated using Darcy's law, a particle was numerically injected from the center of each hexahedral element on the bed surface, and its flow path and residence time were calculated with the particle tracking method. Consequently, for each hexahedral subarea, the exchange flux and residence time were assessed and used to evaluate equations (5) and (6), which were solved with an external subroutine.

4. Experiments

[35] We ensured uniform flow by checking that the water elevations were nearly constant at selected points having one-wavelength spacing. Constant elevations ensure that backwater or acceleration effects at the end of the flume were not present and that the flume was simulating a section of an infinite sequence of pool-riffle units. Then, we siphoned the minipiezometer tubes with a syringe to remove air bubbles from each line.

[36] The recirculation time of the system was calculated, and the tracers were added at a constant rate over the time required for a single recirculation. This was done to ensure that no strong longitudinal gradients were formed. The tracer was poured into the downstream end of the flume in the highly turbulent section before the water dropped into the sump and entered the pump inlet. This location was chosen to ensure full mixing of the solute with the water before it entered the flume. At the end of each run, the sediment was cleaned by replacing all of the water in the system with clean water and letting the pump run, rinsing the sediment until the background conductivity values were reached. The cleaning process lasted more than four hours after the end of each experiment.

5. Results and Discussion

5.1. Pressure Distribution

[37] Figure 8 shows an example of longitudinal and lateral variations in both the near-bed and hydrostatic pressures over the pool-riffle unit. The tails of the pools (XS 26 and 49) and the stoss side of the riffle (XS 29–32) tend to have higher near-bed pressure than both the lee side
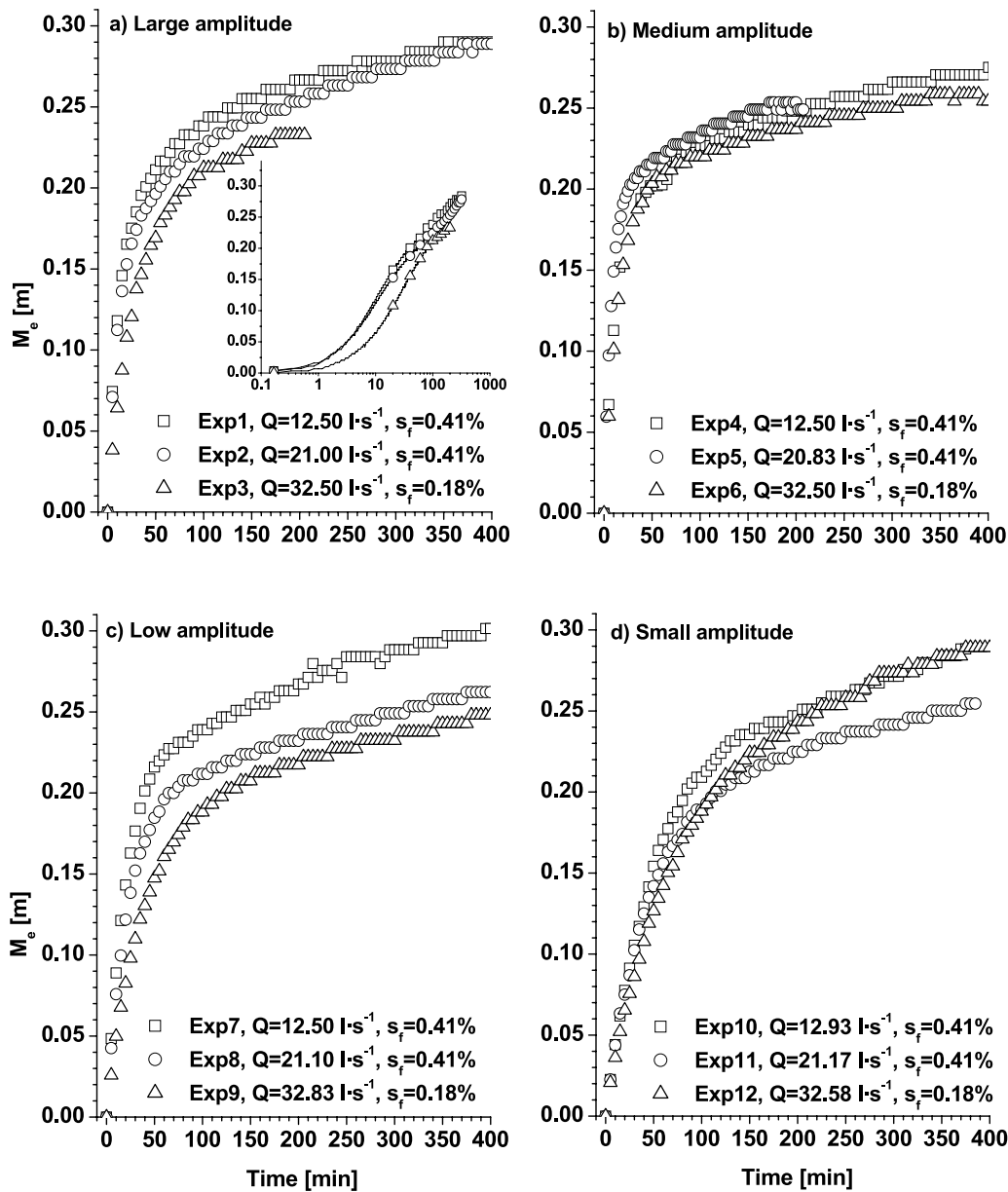
Figure 9. Average effective depth of fluorescein penetration per unit water surface area (M_e) for increasing discharge grouped by bed form amplitude (a–d) from largest to smallest.

of the riffle (XS 38) and the head of the pool (XS 41–44) (see Figure 6 for cross section locations and channel topography). Lateral pressure variations are also present along channel cross sections, creating a three-dimensional pressure distribution. (See Figure 8: Lateral variations for each cross section are shown from left to right across the channel, looking downstream, with empty spaces indicating exposed piezometers along the dry part of the bar. Sample locations are shown in Figure 6.)

[38] In general, the hydrostatic and near-bed pressure profiles are similar (Figure 8), although local discrepancies are observed, particularly for low discharges and high-amplitude bed forms. For those conditions, the area around the riffle crest had much higher Froude numbers than the pool, creating a zone of high instability (hydraulic jumps or surface waves) as shown in Figures 1 and 5. At low flows ($Q = 12.5-21 \, l\,s^{-1}$), as the water entered the pool, it tended

to be wavy over the outer side of the pool and smooth over the inner portion of the pool close to the bar (Figures 1 and 5). The unsteady, pulsating movement of the surface waves can cause measurement errors of the surface elevation and may partially explain the observed discrepancy between hydrostatic and near-bed pressures during low flows. Moreover, the area below the surface waves was characterized by vortices and eddies with strong dynamic head at the boundary, generating a near-bed pressure distribution different from that described by the local water elevation. Differences between hydrostatic and near-bed pressures may also be due to small surface irregularities (e.g., microtopography of particle clusters) as observed by *Packman et al.* [2004] that create dynamic pressure variations that are detected by the near-bed piezometers, but are too small to substantially affect water surface elevations and consequent calculations of hydrostatic pressure. Nevertheless, regions

of higher near-bed pressures were also characterized by higher static pressure (Figure 8).

5.2. Hyporheic Exchange

5.2.1. Exchange Depth

[39] Figure 9 shows hyporheic exchange expressed as the effective depth of solute penetration as a function of time ($M_e(t)$), which is calculated from the observed, normalized, in-stream concentration $C^*(t) = C(t)/C_0$ with the following expression

$$M_e = \frac{V_w(1 - C^*)}{W_s \varphi C^*} \quad (8)$$

where V_w is the recirculating volume of water, W_s the planar (horizontally projected) water surface area, and φ the porosity of the sediment, which was assumed constant and equal to 0.34. Hence M_e is the effective average depth of solute penetration per unit area of the water surface. We used this quantity in order to compare results from experiments with different recirculation volumes and different water surface areas. In pool-riffle systems, water surface area and wetted bathymetry are functions of bed form geometry, and change with discharge until the bars are entirely submerged.

[40] The inset of Figure 9a, which is typical of all the data, expresses the results in terms of the natural log of time to better show the behavior of the hyporheic exchange, which happened in two stages: a rapid exchange that characterizes the initial part of the experiments (nonlinear part of the curve), and a second stage of slow mixing (tail of the curve where the temporal increase in penetration depth is approximately linear). Most of the mixing occurred in this first stage, with a 15%–20% decrease in in-stream solute concentration. This mixing was rapid (occurring in the first 30–60 min), and was predominated by hyporheic exchange across the riffles and bars, where short and fast pathlines are located (section 5.2.2). The second stage of exchange had a roughly constant rate of mixing and penetration that persisted for the remainder of each experiment. However, the duration of the experiments was not long enough to reach total mixing of surface and pore water.

[41] The presence of two consecutive stages of mixing characterized by fast and slow rates of exchange produce two volumes within the hyporheic zone: a shallow one that is strongly coupled to the surface water due to fast rates of exchange, and a deeper layer that experiences slower rates of exchange and therefore is less coupled with the in-stream water. This stratification was also observed by *Packman et al.* [2000] and *Zaramella et al.* [2003] and may generate flux gradients, which could affect habitat selection. A potential cause for the two phases of hyporheic flow (Figure 9 inset) and the vertical stratification of rates of exchange is discussed further in section 5.2.2.

[42] The remaining results shown in Figure 9 are grouped by bed form amplitude to examine the effect of discharge on hyporheic exchange for a given bed form amplitude. Except for the medium amplitude bed form, we find that increasing the discharge causes a decrease in specific hyporheic exchange (smaller penetration depths, M_e, with greater discharge) (Figures 9a, 9c, and 9d, although only for the initial phase of Figure 9d). This result for pool-riffle

channels contrasts with those observed for dune-ripple morphologies [*Elliott and Brooks*, 1997a; *Packman and Bencala*, 1999; *Marion et al.*, 2002] and is likely due to differences in relative submergence of the bed forms and resultant differences in hydraulics between these two channel types. In dune-ripple channels, the bed forms are entirely submerged and are small compared to the water depth, with a water surface profile that is minimally influenced by local bed form topography and roughness. Because the relative submergence is high in dune-ripple channels, the water surface profile is relatively smooth, minimizing spatial variations in water surface topography and its influence on flow depth and static pressure. For such channels, the pressure profile strongly depends on the dynamic pressure, which is a function of mean flow velocity raised to the second power [*Vittal et al.*, 1977], and which increases with greater discharge. Hence hyporheic flow tends to increase with discharge in dune-ripple channels, contrary to what we observe for our pool-riffle experiments (Figure 9). In pool-riffle channels, the relatively large size and three-dimensional structure of bed forms strongly influence the water surface topography and consequent flow depth and static pressure. For low discharges or large bed form amplitudes, the water surface meanders around the gravel bars and exhibits water surface topography that varies both laterally and longitudinally, enhancing the spatial divergence of pressure and the magnitude of hyporheic exchange (e.g., Figures 1 and 5). As discharge increases and bed topography becomes submerged, the spatial variations in the water surface topography and near bed pressure decline, decreasing the hyporheic exchange.

[43] This effect of increasing hyporheic flux with lowering discharge in pool-riffle channels likely has a positive impact on mountain river ecosystems because low flows with partially submerged bed forms are common. Consequently, river-pore water interaction remains intense for most of the year. Moreover, low discharges are typical in snowmelt-dominated basins of the western United States during the fall and winter seasons when embryos of several salmonid species are typically incubating within streambed gravels [*Meehan and Bjornn*, 1991]. These low discharges increase hyporheic flow, which oxygenates the sediment advectively, and creates favorable conditions for embryo survival during this period of the year.

[44] The fact that hyporheic exchange is not always influenced by discharge (Figure 9b) and that the relationship with discharge does not persist at later stages of the experiments for the small-amplitude bed form (Figure 9d), suggests that other factors may also be important. We examine some of these factors (e.g., groundwater slope and depth of alluvium) in detail elsewhere [*Tonina*, 2005].

[45] In Figure 10, we present the results grouped by discharge and slope, showing the effect of bed form amplitude on hyporheic exchange. Contrary to expectations, hyporheic exchange (M_e) does not always decrease with lower bed form amplitude.

[46] The above results indicate that bed form amplitude is not the only control on hyporheic exchange. Rather, there is a complex interaction between discharge and bed form topography that drives flow regime (wetted perimeter, water surface profile, depth, and near-bed pressure) and the
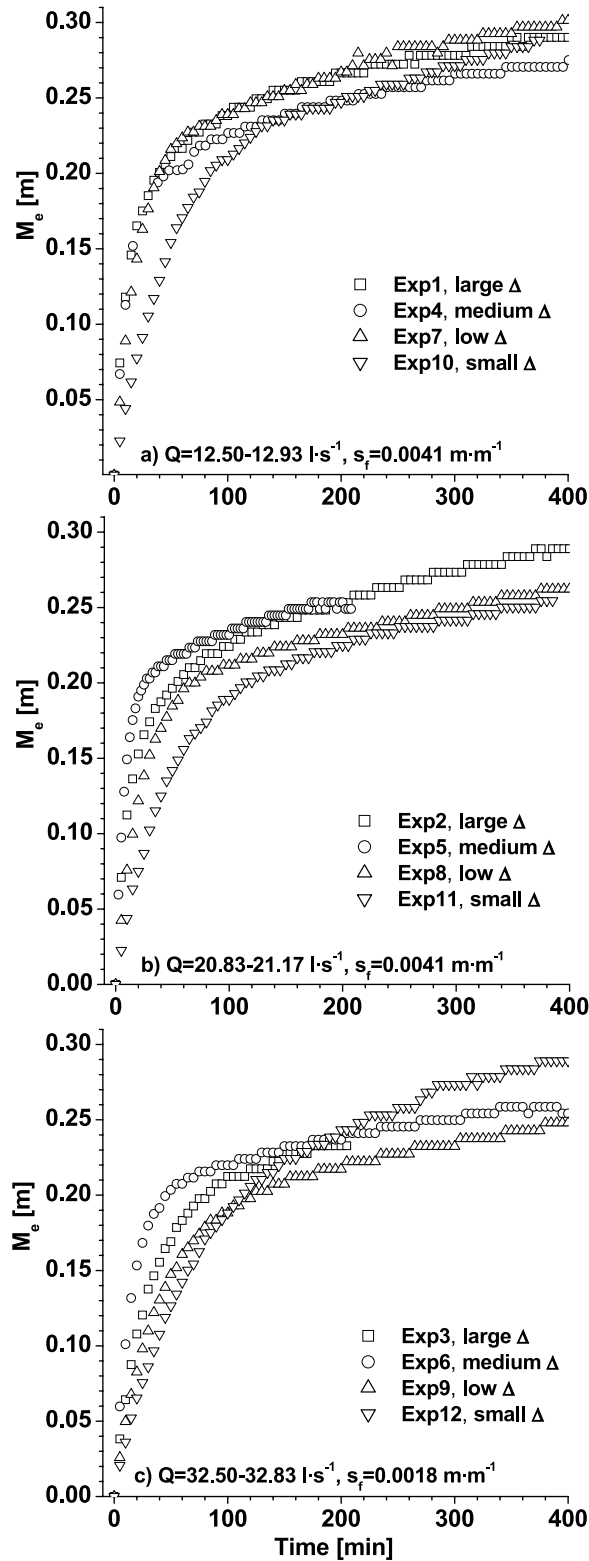
Figure 10. Average effective depth of fluorescein penetration per unit water surface area (M_e) for large- to small-amplitude bed forms grouped by constant values of (a–c) discharge and slope.

consequent magnitude and pattern of hyporheic exchange. Moreover, the hyporheic exchange observed in our pool-riffle channels was stronger than that previously reported for sand bed experiments. This is due to the high permeability of our coarse-grained sediment and the strong head gradients created by pool-riffle topography and low relative submergence, suggesting that the river and the near surface aquifer are closely coupled by active hyporheic flow in coarse-grained mountain rivers. These results agree with previous field studies of coarse-grained channels, where it was observed that the large-scale bed form complexity of mountain streams can create significant elevation differences across the channel that generate substantial hyporheic flow [e.g., *Wondzell and Swanson*, 1996; *Haggerty et al.*, 2002; *Gooseff et al.*, 2006].

5.2.2. Flow Paths

[47] We can follow the hyporheic exchange of the solute into the sediment using pathlines to trace the trajectories of particles through the subsurface. Figure 11 shows predicted pathlines for Experiment 4 (medium-amplitude bed form, low discharge). The pathlines show a complex flow field, as observed in field studies of other channel types [*Kasahara and Wondzell*, 2003; *Storey et al.*, 2003; *Cardenas et al.*, 2004].

[48] Our predictions indicate that there was an intense flux across the riffle crest and at the head of the downstream pool in Experiment 4. Figure 11 also shows that hyporheic flow occurs in both downstream and upstream directions, depending on local head gradients (e.g., lower-right corner of Figure 11). The pathlines also show that the depth of hyporheic exchange is spatially variable, as is the flux of hyporheic flow (indicated by the distance between pathlines). High fluxes are localized around the riffle crest were pathlines converge, while lower-intensity flows (widely spaced pathlines) occur around the pool. Heterogeneous sediment would enhance the complexity of the results by adding a spatially varying hydraulic conductivity field to the three dimensionality of the flow and bed form geometry [*Salehin et al.*, 2004; *Cardenas et al.*, 2004].

[49] The heterogeneity of the flow path distribution may explain the two-stage hyporheic exchange discussed earlier (Figure 9 inset and section 5.2.1). The transition from nonlinear to linear exchange may occur when the faster flows at the riffle and bar head have completely mixed the surface water and pore water in those zones, after which the exchange within the channel is dominated by the slower, deeper, pore water mixing (e.g., beneath the bars), where fluxes are less intense as indicated by more widely spaced pathlines (Figure 11).

[50] The hyporheic exchange in the riffle area is particularly important for salmonid ecology. The predicted exchange across the riffle is characterized by strong downwelling on the upstream side of the riffle, and upwelling on the downstream side (where flow paths converge) (Figure 11), as typically observed in the field [*Baxter and Hauer*, 2000; *Geist*, 2000]. Salmonids preferentially spawn in this zone [*Crisp and Carling*, 1989; *Bjornn and Reiser*, 1991] and may be attracted to the strong hyporheic circulation through the riffle [*Geist*, 2000]. Additionally, this circulation cell is important for oxygenating buried salmonid embryos, removing metabolic waste, and sweeping
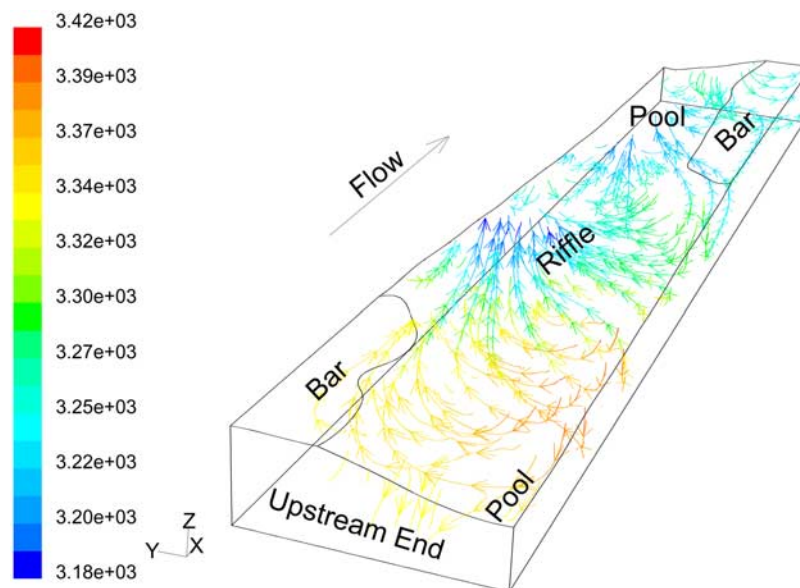
Figure 11. Predicted hyporheic pathlines for Exp4 (medium-amplitude bed form, low discharge), colored by total pressure (Pascals). All pathlines originate from the surface.

away fine sediment that would clog gravel pores and decrease survival to emergence [*Bjornn and Reiser*, 1991].

[51] Predicted pathlines could also be used to define the hyporheic volume hydraulically, as suggested by *Cardenas et al.* [2004]. In this approach, the hyporheic zone would be delineated by the surface enveloping the pathlines, recognizing that the solute concentration and strength of hyporheic exchange vary within this volume.

5.2.3. Comparison With Exchange Models

[52] In Figure 12, we compare the measured hyporheic exchange to that predicted from two models: *Elliott and Brooks'* [1997a] model for two-dimensional dune-like bed forms as modified by *Packman et al.* [2000] for a finite depth of alluvium, and the three-dimensional pumping model presented in section 2. We also compare results for the three-dimensional model driven by the near-bed pressure distribution versus that of the hydrostatic pressure.

[53] The three-dimensional pumping model driven by the near-bed pressure predicts the overall hyporheic exchange reasonably well (Figure 12), indicating that surface-subsurface exchange in pool-riffle channels is predominantly driven by bed form−induced advection resulting from the interaction between in-stream flow and bed form topography.

[54] When the hydrostatic pressure is used as a surrogate for the near-bed pressure, the model does not perform well for large- and medium-amplitude bed forms or low discharges, underestimating the exchange (Figure 12, plots Exp1, Exp2, Exp4, and Exp5). However, we find that the performance of the hydrostatic model improves when the discharge is increased or the bed form amplitude is reduced (Figure 12, moving from left to right plots of a given row, or top to bottom of a given column). For conditions of low flow and high bed form amplitude, substantial dynamic pressure variations exist, which are not accounted for by the hydrostatic pressure, making it a poor proxy for the near-bed pressure. Furthermore, in these cases, the water surface exhibited unsteady surface waves above the high-velocity

core in the vicinity of the riffle, which made the water surface profile measurements difficult to make and more prone to error (Figures 1 and 5).

[55] For the two-dimensional pumping exchange model [*Elliott and Brooks*, 1997a; *Packman et al.*, 2000], we defined the depth of alluvium, d_b, corresponding to the average sediment thickness in the flume, as the saturated volume of sediment divided by the bed surface area. Additionally, we assumed two-dimensional bed forms having amplitude and wavelength values equivalent to our pool-riffle bed forms (Table 2). Results show that the two-dimensional model underestimates the solute exchange between surface and subsurface water in all experiments (Figure 12). These differences are expected because of application of a two-dimensional model to a three-dimensional problem of hyporheic exchange in a pool-riffle channel with alternate bars. The two-dimensional model assumes a downstream sinusoidal pressure distribution that is appropriate for two-dimensional dunes, but not pool-riffle topography. Furthermore, it assumes that the longitudinal head variation is constant along the cross-channel direction, which is not the case in pool-riffle channels with alternate bars. Flow over pool-riffle topography creates a cross-channel head profile (Figure 8), the gradient of which varies in the downstream direction (Figure 5), adding complexity that enhances the exchange (Figure 11).

[56] An additional factor that may be characteristic of coarse bed rivers and that may cause error in both the two- and three-dimensional models is the presence of non-Darcy hyporheic flow [*Packman et al.*, 2004]. Reynolds numbers greater than unity indicate flow conditions for which Darcy's law does not hold without correction for inertial accelerations and momentum exchange with the surface flow field [*Nagaoka and Ohgaki*, 1990; *Shimizu et al.*, 1990]. *Packman et al.* [2004] examined hyporheic exchange through porous gravel beds having a dune-like morphology and found that the modified Elliot and Brooks model [*Packman et al.*, 2000] did not perform well for two
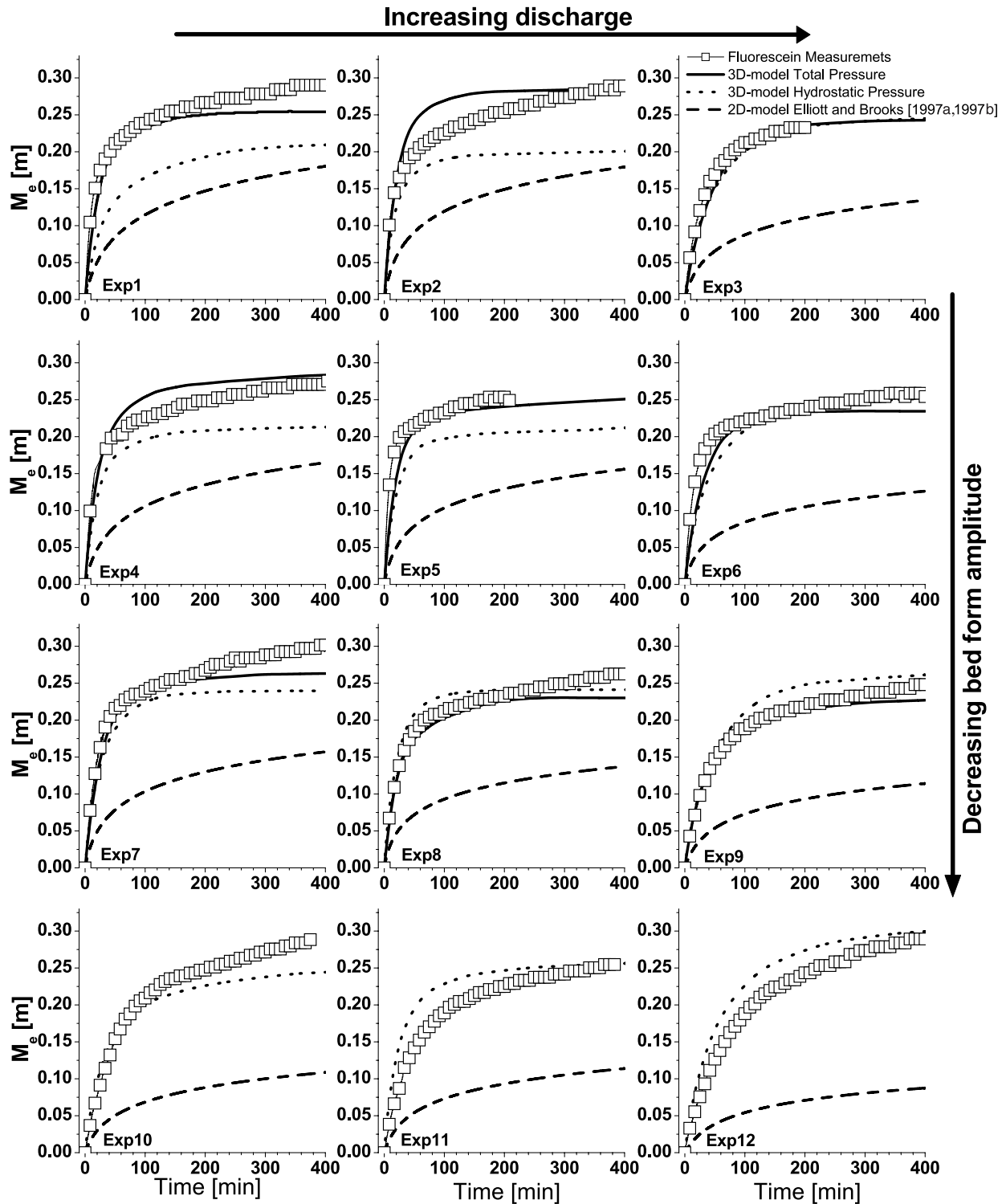
Figure 12. Observed versus predicted hyporheic exchange expressed in terms of average solute depth per unit water surface area (M_e) for each experiment. Discharge increases across the plots from left to right, and bed form amplitude decreases across the plots from top to bottom (Tables 1 and 2). Values of total near-bed head were not measurable in the last set of experiments (Exp10 to Exp12).

reasons: non-Darcy flow in the near-surface sediment volume, and the presence of small, surface irregularities that generated dynamic pressure variations.

[57] We recognize that non-Darcy flow may have been present in the weak armor layer that formed during our experiments, but preliminary dye tracer experiments indicated that its effect was limited to the near-surface layer and is likely minimal in the overall exchange. Nevertheless, non-Darcy flow may partially explain some of the discrep-

ancy between our predicted and observed values of hyporheic exchange.

6. Conclusion

[58] We present a three-dimensional modification of *Elliott and Brooks'* [1997a] pumping exchange model to predict the hyporheic flow in gravel pool-riffle channels, in which bed topography variations are captured and the observed pressure profile at the bed surface drives hyporheic flow. Comparison between modeled and measured exchange shows agreement, suggesting that hyporheic exchange in these channels is predominantly driven by bed form–induced advection modulated by discharge and topographic submergence. Bed forms affect both the near-bed pressure and the surface area available for hyporheic exchange at a given flow. However, a primary finding of our study is that bed form amplitude in pool-riffle channels is not the only key factor for driving hyporheic exchange; rather, there is a complex interaction between discharge and bed form topography that drives flow regime (wetted perimeter, water surface profile, depth, and near-bed pressure) and the consequent magnitude and pattern of hyporheic exchange.

[59] We find that the two-dimensional pumping exchange model for sand bed rivers with dune-like bed forms (*Elliott and Brooks* [1997a, 1997b] as modified by *Packman et al.* [2000]) does not perform well in gravel bed rivers with pool-riffle morphology. For dune-ripple morphologies, the relative submergence of the bed forms (flow depth relative to bed form amplitude) is high and the water surface is not strongly affected by the bed forms. Changes in pressure are predominantly due to the dynamic pressure, which, in that case, can be represented by a simple, two-dimensional, downstream, sinusoidal pattern [*Elliott and Brooks*, 1997a]. In contrast, in pool-riffle channels, the water surface responds to bed form shape and amplitude because of low relative submergence, and the near-bed pressure profile is strongly influenced by spatial and temporal changes in water surface elevation. Moreover, at low flow, unstable standing waves downstream of the riffle crest influence the pressure distribution and hyporheic exchange. These three-dimensional effects were not included in *Elliott and Brooks'* [1997a] model for hyporheic exchange under two-dimensional dunes.

[60] We also find that the hydrostatic pressure can be substituted for the total near-bed pressure in the three-dimensional pumping exchange model under conditions of high discharge and/or low-amplitude bed forms. However, it does not work well for low flows and large-amplitude bed forms, where strong surface waves form, below which the near-bed pressure is no longer hydrostatic. Nevertheless, the hydrostatic pressure may provide a useful first-order solution of hyporheic exchange in field studies of pool-riffle channels where near-bed pressure measurements are difficult to make [e.g., *Baxter and Hauer*, 2000].

[61] Results of this study show that pool-riffle channels not only have complex surface hydraulics, with spatially varying flow depths and velocities that change with discharge, but they also have corresponding spatial and temporal complexity of hyporheic flow, creating a highly diverse environment that may cause benthic species to adapt to seasonal variations in flow. Because of these physical heterogeneities, it is important to have a holistic perspective that links in-stream and hyporheic flows in studies of solute transport and aquatic habitat in pool-riffle channels.

Notation

A [m^2]	cross-sectional flow area.
C [kg m^{-3}]	solute concentration.
C_0 [kg m^{-3}]	initial solute concentration.
C^* [$-$]	normalized concentration defined as $C(t)/C_0$.
d_b [m]	depth of alluvium.
H [m]	energy head defined as total pressure plus elevation head.
k [m s^{-1}]	hydraulic conductivity.
M_e [m]	effective depth of solute penetration per unit area of the water surface, $M_e = V_w(1 - C^*)/(W_s \varphi C^*)$.
m_e [m]	average depth of solute penetration per unit area of the water surface, independent of sediment porosity ($M_e \varphi$), equation (5).
$\mathbf{n}$ [$-$]	unit vector orthogonal to the sediment surface (positive pointing inward).
P_H [m]	wetted perimeter.
Q [m^3 s^{-1}]	in-stream discharge.
q [m s^{-1}]	local downwelling flux.
$\overline{q}$ [m s^{-1}]	average downwelling flux.
R_T [$-$]	cumulative distribution function of the residence time.
RTD [$-$]	flux-weighted average residence time distribution.
s_f [m m^{-1}]	flume and energy slope.
T [s]	residence time associated with an injection point.
t [s]	elapsed time since injection.
t_0 [s]	injection time equal to 0.
$\mathbf{u}$ [m s^{-1}]	Darcy velocity vector.
$\mathbf{u}_b$ [m s^{-1}]	Darcy velocity vector at the sediment surface.
V_w [m^3]	total water volume present in the system except for pore water.
W_p [m^2]	three-dimensional surface area of wetted topography.
W_s [m^2]	planar (horizontally projected) water surface area.
$\mathbf{x}$ [m]	coordinate vector.
x [m]	position along the longitudinal direction of the flume.
y [m]	position along the cross-sectional direction of the flume.
Δ [m]	bed form amplitude (residual depth).
λ [m]	bed form wavelength.
φ [m^3 m^{-3}]	sediment porosity.
τ [s]	dummy time variable of integration.

References

Baxter, C. V., and R. F. Hauer (2000), Geomorphology, hyporheic exchange, and selection of spawning habitat by bull trout (*Salvelinus confluentus*), *Can. J. Fish. Aquat. Sci.*, *57*, 1470–1481.

Bencala, K. E., and R. A. Walters (1983), Simulation of solute transport in a mountain pool-and-riffle stream: A transient storage model, *Water Resour. Res.*, *19*, 718–724.

Bjornn, T. C., and D. W. Reiser (1991), Habitat requirements of salmonids in streams, in *Influences of Forest and Rangeland Management on Salmonid Fishes and Their Habitats*, *Am. Fish. Soc. Spec. Publ. 19*, edited by W. R. Meehan, pp. 83–138, Bethesda, Md.

Buffington, J. M., and D. R. Montgomery (1999), Effects of hydraulic roughness on surface textures of gravel-bed rivers, *Water Resour. Res.*, *35*, 3507–3521.

Buffington, J. M., T. E. Lisle, R. D. Woodsmith, and S. Hilton (2002), Controls on the size and occurrence of pools in coarse-grained forest rivers, *River Res. Appl.*, *18*, 507–531.

Buffington, J. M., R. D. Woodsmith, D. B. Booth, and D. R. Montgomery (2003), Fluvial processes in Puget Sound rivers and the Pacific northwest, in *Restoration of Puget Sound Rivers*, edited by D. R. Montgomery et al., pp. 46–78, Univ. of Wash. Press, Seattle.

Buffington, J. M., D. R. Montgomery, and H. M. Greenberg (2004), Basin-scale availability of salmonid spawning gravel as influenced by channel type and hydraulic roughness in mountain catchments, *Can. J. Fish. Aquat. Sci.*, *61*, 2085–2096, doi:10.1139/F04-141.

Cardenas, B. M., J. F. Wilson, and V. A. Zlotnik (2004), Impact of heterogeneity, bed forms, and stream curvature on subchannel hyporheic exchange, *Water Resour. Res.*, *40*, W08307, doi:10.1029/2004WR003008.

Carling, P. (1992), In-stream hydraulics and sediment transport, in *The Rivers Handbook*, edited by P. Carlow and G. E. Petts, pp. 101–125, Blackwell, Malden, Mass.

Carling, P., and H. G. Orr (2000), Morphology of riffle-pool sequences in the River Severn, England, *Earth Surf. Processes Landforms*, *25*, 369–384.

Colombini, M., G. Seminara, and M. Tubino (1987), Finite-amplitude alternate bars, *J. Fluid Mech.*, *181*, 213–232.

Cooper, A. C. (1965), The effect of transported stream sediments on the survival of sockeye and pink salmon eggs and alevin, *Int. Pac. Salmon Fish. Comm. Bull.*, *18*.

Crisp, D. T., and P. A. Carling (1989), Observations on siting, dimensions, and structure of salmonid redds, *J. Fish Biol.*, *34*, 119–134.

Dagan, G. (1979), The generalization of Darcy's law for nonuniform flow, *Water Resour. Res.*, *15*, 1–7.

Dietrich, W. D., and P. J. Whiting (1989), Boundary shear stress and sediment transport in river meanders of sand and gravel, in *River Meandering*, *Geophys. Monogr. Ser.*, vol. 12, edited by S. Ikeda and G. Parker, pp. 1–50, AGU, Washington D. C.

Edwards, R. T. (1998), The hyporheic zone, in *River Ecology and Management: Lessons From the Pacific Coastal Ecoregion*, edited by R. J. Naiman and R. E. Bilby, pp. 399–429, Springer, New York.

Elliott, A., and N. H. Brooks (1997a), Transfer of nonsorbing solutes to a streambed with bed forms: Laboratory experiments, *Water Resour. Res.*, *33*, 137–151.

Elliott, A., and N. H. Brooks (1997b), Transfer of nonsorbing solutes to a streambed with bed forms: Theory, *Water Resour. Res.*, *33*, 123–136.

Freeze, R. A., and J. A. Cherry (1979), *Groundwater*, 604 pp., Prentice-Hall, Upper Saddle River, N. J.

Geist, D. R. (2000), Hyporheic discharge of river water into fall chinook salmon (*Oncorhynchis tshawytscha*) spawning areas in the Hanford Reach, Columbia River, *Can. J. Fish. Aquat. Sci.*, *57*, 1647–1656.

Gibert, J., J. A. Stanford, M. J. Dole-Oliver, and J. V. Ward (1994), Basic attributes of groundwater ecosystems and prospects for research, in *Groundwater Ecology*, edited by J. Gilbert, D. L. Danielpol, and J. A. Standford, pp. 8–40, Elsevier, New York.

Gooseff, M. N., J. K. Anderson, S. M. Wondzell, J. LaNier, and R. Haggerty (2006), A modelling study of hyporheic exchange pattern and the sequence, size, and spacing of stream bedforms in mountain stream networks, Oregon, USA, *Hydrol. Processes*, *19*, 2915–2929.

Haggerty, R., S. M. Wondzell, and M. A. Johnson (2002), Power-law residence time distribution in hyporheic zone of a 2nd-order mountain stream, *Geophys. Res. Lett.*, *29*(13), 1640, doi:10.1029/2002GL014743.

Harvey, J. W., and K. E. Bencala (1993), The effect of streambed topography on surface-subsurface water exchange in mountain catchments, *Water Resour. Res.*, *29*, 89–98.

Hassanizadeh, M. S., and W. G. Gray (1979), General conservation equations for multi-phase systems: 1. Averaging procedure, *Adv. Water Resour.*, *2*, 131–144.

Hassanizadeh, M. S., and W. G. Gray (1987), High velocity flow in porous media, *Transp. Porous Media*, *2*, 521–531.

Ho, R. T., and L. W. Gelhar (1973), Turbulent flow with wavy permeable boundaries, *J. Fluid Mech.*, *58*, 403–414.

Kasahara, T., and S. M. Wondzell (2003), Geomorphic controls on hyporheic exchange flow in mountain streams, *Water Resour. Res.*, *39*(1), 1005, doi:10.1029/2002WR001386.

Keller, E. A., and W. N. Melhorn (1978), Rhythmic spacing and origin of pools and riffles, *Geol. Soc. Am. Bull.*, *89*, 723–730.

Kondolf, M. G., and G. M. Wolman (1993), The size of salmonid spawning gravel, *Water Resour. Res.*, *29*, 2275–2285.

Lanzoni, S., and M. Tubino (1999), Grain sorting and bar instability, *J. Fluid Mech.*, *393*, 149–174.

Leopold, L. B., M. G. Wolman, and J. P. Miller (1964), *Fluvial Processes in Geomorphology*, 522 pp., W. H. Freeman, New York.

Levy, D. A., and T. L. Slaney (1993), A review of habitat capability for salmon spawning and rearing, report, 48 pp., B. C. Resour. Inventory Comm., Vancouver, B. C., Canada.

Lisle, T. E., and S. Hilton (1992), The volume of fine sediment in pools: An index of sediment supply in gravel-bed streams, *Water Resour. Bull.*, *28*, 371–382.

Marion, A., M. Bellinello, I. Guymer, and A. I. Packman (2002), Effect of bed form geometry on the penetration of nonreactive solutes into a streambed, *Water Resour. Res.*, *38*(10), 1209, doi:10.1029/2001WR000264.

Meehan, W. R., and T. C. Bjornn (1991), Salmonid distributions and life histories, in *Influences of Forest and Rangeland Management on Salmonid Fishes and Their Habitats*, *Am. Fish. Soc. Spec. Publ. 19*, edited by W. R. Meehan, pp. 47–82, Bethesda, Md.

Mendoza, C., and D. Zhou (1992), Effects of porous bed on turbulent stream flow above bed, *J. Hydraul. Eng.*, *118*, 1222–1240.

Moir, H. J., C. N. Gibbins, C. Soulsby, and J. Webb (2004), Linking channel geomorphic characteristics to spatial patterns of spawning activity and discharge use by Atlantic salmon (*Salmo salar* L.), *Geomorphology*, *60*, 21–35.

Montgomery, D. R. (2003), *King of Fish: The Thousand-Year Run of Salmon*, 290 pp., Westview, Boulder, Colo.

Montgomery, D. R., and J. M. Buffington (1997), Channel-reach morphology in mountain drainage basins, *Geol. Soc. Am. Bull.*, *109*, 596–611.

Montgomery, D. R., E. M. Beamer, G. R. Pess, and T. P. Quinn (1999), Channel type and salmonid spawning distribution and abundance, *Can. J. Fish. Aquat. Sci.*, *56*, 377–387.

Nagaoka, H., and S. Ohgaki (1990), Mass transfer mechanism in a porous riverbed, *Water Res.*, *24*, 417–425.

Nehlsen, W., J. E. Williams, and J. A. Lichatowich (1991), Pacific salmon at the crossroads: Stocks at risk from California, Oregon, Idaho, and Washington, *Fisheries*, *16*, 4–21.

Packman, A. I., and K. E. Bencala (1999), Modeling methods in study of surface-subsurface hydrological interactions, in *Stream and Ground Waters*, edited by J. B. Jones and P. J. Mulholland, pp. 45–80, Elsevier, New York.

Packman, A. I., N. H. Brooks, and J. J. Morgan (2000), A physicochemical model for colloid exchange between a stream and a sand streambed with bed forms, *Water Resour. Res.*, *36*, 2351–2361.

Packman, A. I., M. Salehin, and M. Zaramella (2004), Hyporheic exchange with gravel beds: Basic hydrodynamic interactions and bedform-induced advective flows, *J. Hydraul. Eng.*, *130*, 647–656.

Prestegaard, K. L. (1983), Bar resistance in gravel bed streams at bankfull stage, *Water Resour. Res.*, *19*, 472–476.

Ruff, J. F., and L. W. Gelhar (1972), Turbulent shear flow in porous boundary, *J. Eng. Mech. Div. Am. Soc. Civ. Eng.*, *98*, 975–991.

Salehin, M., A. I. Packman, and M. Paradis (2004), Hyporheic exchange with heterogeneous streambeds: Laboratory experiments and modeling, *Water Resour. Res.*, *40*(11), W11504, doi:10.1029/2003WR002567.

Savant, A. S., D. D. Reible, and L. J. Thibodeaux (1987), Convective transport within stable river sediments, *Water Resour. Res.*, *23*, 1763–1768.

Shimizu, Y., T. Tsujimoto, and H. Nakagawa (1990), Experiments and macroscopic modeling of flow in highly permeable porous medium under free-surface flow, *J. Hydraul. Eng.*, *8*, 69–78.

Stanford, J. A., and J. V. Ward (1993), An ecosystem perspective of alluvial rivers: Connectivity and the hyporheic corridor, *J. N. Am. Benthol. Soc.*, *12*, 48–60.

Storey, R. G., K. W. F. Howard, and D. D. Williams (2003), Factors controlling riffle-scale hyporheic exchange flows and their seasonal changes in gaining stream: A three-dimensional groundwater model, *Water Resour. Res.*, *39*(2), 1034, doi:10.1029/2002WR001367.

Thibodeaux, L. J., and J. D. Boyle (1987), Bedform-generated convective transport in bottom sediment, *Nature*, *325*, 341–343.

Tompson, A. F. B., and L. W. Gelhar (1990), Numerical simulation of solute transport in three-dimensional randomly heterogeneous porous media, *Water Resour. Res.*, *26*, 2451–2462.

Tonina, D. (2005), Interaction between river morphology and intra-gravel flow paths within the hyporheic zone, Ph.D. dissertation, 129 pp., Univ. of Idaho, Boise.

Tubino, M. (1991), Growth of alternate bars in unsteady flow, *Water Resour. Res.*, *27*, 37–52.

Vittal, N., K. G. Ranga Raju, and R. J. Garde (1977), Resistance of two-dimensional triangular roughness, *J. Hydraul. Res.*, *15*, 19–36.

Williams, D. D., and H. B. N. Hynes (1974), The occurrence of benthos deep in the substratum of stream, *Freshwater Biol.*, *4*, 233–256.

Wolman, M. G. (1954), A method of sampling coarse bed material, *Eos Trans. AGU*, *35*, 951–956.

Wondzell, S. M., and F. J. Swanson (1996), Seasonal and storm dynamics of the hyporheic zone of 4th order mountain stream. 2: Nitrogen cycling, *J. N. Am. Benthol. Soc.*, *15*, 20–34.

Wörman, A., A. I. Packman, H. Johansson, and K. Jonsson (2002), Effect of flow-induced exchange in hyporheic zones on longitudinal transport of solutes in streams and rivers, *Water Resour. Res.*, *38*(1), 1001, doi:10.1029/2001WR000769.

Zaramella, M., A. I. Packman, and A. Marion (2003), Application of the transient storage model to analyze advective hyporheic exchange with deep and shallow sediment beds, *Water Resour. Res.*, *39*(7), 1198, doi:10.1029/2002WR001344.

————————————
J. M. Buffington and D. Tonina, Rocky Mountain Research Station, U.S. Forest Service, Boise, ID 83702, USA. (dtonina@fs.fed.us)